

MOVPE studies of zincblende GaN on 3C-SiC/Si(001)

T.J. Wade^a, A. Gundimeda^a, M.J. Kappers^{a,*}, M. Frentrop^a, S.M. Fairclough^a, D.J. Wallis^{a,b}, R. A. Oliver^a^a University of Cambridge, Department of Materials Science and Metallurgy, 27 Charles Babbage Road, Cambridge CB3 0FS, United Kingdom^b University of Cardiff, Centre for High Frequency Engineering, 5 The Parade, Newport Road, Cardiff CF24 3AA, United Kingdom

ARTICLE INFO

Communicated by Tanya Paskova

Keywords:

- A1. Atomic force microscopy
- A1. X-ray diffraction
- A1. Scanning-transmission electron microscopy
- A1. Phase purity
- A3. Metalorganic vapour-phase epitaxy
- B1. Cubic zincblende GaN

ABSTRACT

Cubic zincblende GaN films were grown by metalorganic vapour-phase epitaxy on 3C-SiC/Si (001) templates and characterized using Nomarski optical microscopy, atomic force microscopy, X-ray diffraction, and transmission-electron microscopy. In particular, structural properties were investigated of films where the growth temperature of a GaN epilayer varied in the range of 830 °C to 910 °C and the gas-phase V/III-ratio varied from 15 to 1200 at a constant reactor pressure of 300 Torr. It was observed that with increasing epi temperature at a constant V/III-ratio of 76, the film surface consisted of micrometer-sized elongated features aligned along [1–10] up to a temperature of 880 °C. The zincblende phase purity of such samples was generally high with a wurtzite fraction of less than 1%. When grown above 880 °C the GaN surface morphology degraded and the zincblende phase purity reduced as a result of inclusions with the wurtzite phase. A progressive narrowing of the 002 reflection with increasing epi growth temperature suggested an improvement of the film mosaicity. With increasing V/III-ratio at a constant growth temperature of 880 °C, the film surface formed elongated features aligned along [1–10] at V/III values between 38 and 300 but the morphology became granular at both lower and higher V/III values. The zincblende phase purity is high at V/III values below 300. A slight broadening of the 002 X-ray diffraction reflection with increasing V/III-ratio indicated a small degradation of mosaicity. Scanning electron diffraction analyses of cross-sectional transmission-electron micrographs taken of a selection of samples illustrated the spatial distribution, quantity and structure of wurtzite inclusions within the zincblende GaN matrix. Within the limits of this study, the optimum epilayer growth conditions at a constant pressure of 300 Torr were identified to be at a temperature around 860 °C to 880 °C and a V/III-ratio in the range of 23 to 76, resulting in relatively smooth, zincblende GaN films without significant wurtzite contamination.

1. Introduction

Compared to the scientific and commercial successes achieved with hexagonal wurtzite (wz-) III-nitrides, the advances made since the early 1990's on the subject of cubic zincblende GaN (zb-GaN) thin films have been modest [1–5]. The small number of zb-GaN growth reports found in the literature concern mostly Molecular Beam Epitaxy (MBE) studies, while a few comprehensive Metalorganic Vapour-Phase Epitaxy (MOVPE) growth studies exist [6–8]. Recently, the growth of zincblende GaN and InGaN received renewed attention [9–12] as a possible route to overcome the so-called “green gap” problem – i.e. the relatively low efficiency of green emitting nitride light emitting diodes (LEDs) compared to blue-emitting devices. Indeed, due to the absence of shear strains, the zincblende phase in the (001) orientation is free of internal electric polarization fields that affect the commonly-used wurtzite c-

plane (0001) orientation [13–15]. Thus, the expectation is that the electron-hole wavefunction overlap in the nonpolar zb-GaN/InGaN quantum well structures is increased compared to that of c-plane wurtzite structures, leading to a faster radiative recombination rate and possibly higher efficiencies [16]. Furthermore, the smaller bandgap of zb-GaN (3.27 eV) compared to that of wz-GaN (3.47 eV) allows for a smaller amount of Indium in the quantum wells, which would be especially advantageous in green-emitting devices. Other device-related properties of zb-GaN such as n- and p-type doping concentrations and carrier mobilities using Si and Mg as dopants, respectively, are largely in line with those reported for wurtzite-type material [17–22], although several recent Mg doping studies of zb-GaN [23–25] reported free hole concentration as high as $6 \times 10^{19} \text{ cm}^{-3}$. Successful n- and p-type doping of zb-GaN was demonstrated by electroluminescence from p-n homo-junctions [23,26–28] and GaN/InGaN heterostructures [29].

* Corresponding author.

E-mail address: mjk30@cam.ac.uk (M.J. Kappers).<https://doi.org/10.1016/j.jcrysgro.2023.127182>

Received 1 November 2022; Received in revised form 3 February 2023; Accepted 14 March 2023

Available online 21 March 2023

0022-0248/© 2023 The Authors. Published by Elsevier B.V. This is an open access article under the CC BY license (<http://creativecommons.org/licenses/by/4.0/>).

A recent resurgence in zb-GaN research activity concerned the growth by MOVPE on nano-patterned Si (001) substrates in which selective area growth is initiated on {111} sidewalls of the patterned V-grooves [9–12]. Thus, the zb-GaN was formed upon coalescence of two, inclined wz-GaN growth fronts, resulting in ridges without wz-GaN surface exposure [12,30]. However, despite the elegance of this selective area overgrowth method, the manufacturing of high-quality, planar zb-GaN films requires epitaxial growth on a more convenient and preferably large-area substrate with a cubic symmetry. In most cases, GaAs (001) or 3C-SiC (001) have been used as the cubic substrate of choice. There have been several efforts of zb-GaN growth on GaAs by MOVPE using 1,1-dimethylhydrazine (DMHy) [31,32] and ammonia [6,33] as N precursors, but due to its higher thermal stability 3C-SiC seems better suited for zb-GaN growth. Furthermore, 3C-SiC has a relatively small lattice mismatch of 3.4% with respect to zb-GaN [34]. Lastly, the current availability of high-quality 3C-SiC/Si (001) substrates of up to 150 mm in diameter makes this the substrate of choice, although, due to the thermal mismatches between GaN, 3C-SiC and Si, strain-management procedures akin to the wz-GaN (0001)/Si (111) technology [35] will need to be developed to allow the growth of zb-GaN films of several micrometers in thickness.

It is clear from the literature that zb-GaN films with high phase purity are difficult to achieve because the zincblende phase is metastable and hence inclusions of the thermodynamically more stable wurtzite phase commonly occur, as do stacking faults on {111} planes. Indeed, the stacking faults (SFs) may be considered as monolayer wurtzite inclusions. Daudin *et al.* [3] and Gerthsen *et al.* [36] identified that zb-GaN MBE growth with high phase purity is mainly governed by three key factors; namely a low substrate roughness, a moderate growth rate, and a V/III gas-phase ratio close to unity. Similarly, a comparison of the different MOVPE conditions used by different groups [6,7,32,37,38] shows that the highest quality films were grown using a standard two-step growth procedure, which included a 20 nm- to 60 nm-thick low-temperature GaN nucleation layer grown at 500 °C to 575 °C with the epilayer grown at a temperature between 800 °C and 950 °C, a V/III-ratio between 12.5 and 1500 and a growth pressure between 20 Torr and 585 Torr. Building on these recommendations from literature and earlier work from our group [8], we report here on the MOVPE growth and characterization of zb-GaN epilayers on 3C-SiC/Si (001) substrates exploring the temperature range between 830 °C and 910 °C and the V/III-ratio range between 15 and 1200 at a reactor pressure of 300 Torr. We found that over a narrow growth window of intermediate values for temperature and V/III-ratio, smooth zincblende films were grown with high phase purity.

2. Experimental method

All samples were grown in a Thomas Swan 6 × 2" close-coupled showerhead MOVPE reactor on 3C-SiC/Si templates. The SiC templates consisted of a circa 3 μm-thick 3C-SiC layer on a Si (001) substrate with a thickness of 0.75 mm or 1.00 mm and a misorientation of 4° towards [110] in order to avoid substrate-induced anti-phase domains (APDs) in the GaN epilayer [8,39]. For the GaN growth, trimethyl gallium (TMG) and ammonia were used as Ga- and N-precursors, while hydrogen was used as the carrier gas. The total gas flow was kept constant at 20 standard litres per minute (slm). The growth procedure comprised of a high-temperature thermal anneal of the substrate followed by a low-temperature nucleation layer deposition and finally the growth of the epilayer proper at high temperature. The temperatures quoted are those recorded by a Laytec EpiTT in-situ optical monitoring system, calibrated against an Al/Si eutectic wafer. The GaN nucleation layer was grown at 600 °C to a thickness of 40 nm while the GaN epilayer thickness was kept constant at 500 nm. Two sample sets (A and B) were prepared in which the variables were the epilayer growth temperature and the V/III-ratio in the gas phase with the reactor pressure maintained at 300 Torr. For set A, the epilayer growth temperature was

varied between 830 °C and 910 °C at a constant V/III-ratio of 76. For set B, the V/III-ratio during epilayer growth at 880 °C was varied between 15 and 1200 by changing the ammonia flow rate at a constant TMG flow rate of 145 μmol/min. All GaN epilayers were intentionally doped with Si to a nominal concentration of mid-10¹⁸ cm⁻³ using silane (50 ppm SiH₄ in H₂).

The phase analysis of the samples was performed by XRD using a PANalytical Empyrean diffractometer equipped with a Cu-Kα₁ source (λ = 1.54056 Å), 2-bounce hybrid monochromator, 1/4°-slit, Eulerian cradle, and a PIXcel solid-state area detector. Reciprocal space maps (RSMs) around the 113 (respectively 1–13) zb-GaN and 1–103 wz-GaN reflections were measured parallel and perpendicular to the miscut direction of the substrate [34,40]. The intensity profiles along the (111) SF streak between the 113 and 1–103 reflections were extracted from the RSMs and subsequently fitted with a maximum of three Pseudo-Voigt functions for the zincblende and wurtzite phases and a third, ill-defined, hence defective phase probably related to a high density of stacking faults. The integrated intensities of the fitted profiles were used to quantify the wurtzite fraction of the GaN epilayers, for which the scattering efficiencies of the 113_{zb} planes and the 1-103_{wz} were assumed to be similar [34]. The residual peak intensity assigned to stacking faults was not quantified in this work. A detailed report on the phase purity analysis by XRD supported by a theoretical description of stacking faults arrays will be the subject of future work. The 002 peak broadening parallel and perpendicular to the sample miscut was measured with a Philips X'Pert diffractometer equipped with an asymmetric 4-crystal Bartels monochromator (λ = 1.54056 Å), 5 × 5 mm² cross slit collimator, Eulerian cradle, and gas proportional point detector without further secondary optics. The intensity profiles of open detector ω-rocking curve scans were fitted with Pseudo-Voigt functions and the FWHM of the fits were used to quantify the reflection broadening.

The surface morphology was measured using a Bruker Dimension Icon Pro AFM in PeakForce Tapping mode, using ScanAsyst-Air-HR probes from Bruker Inc. with nominal tip radii of 2 nm. For each sample four 10 μm × 10 μm large scans (512 × 512 data points each) of different regions were measured with the fast scan direction parallel to [110] (in general parallel to the features' short direction). The free software WSxM 5.0 Develop 9.1 [41] was used for data importation and offset flattening parallel to the fast scan direction. The root mean square (rms) roughness (R) of the epilayers was calculated from 10 μm × 10 μm scans, and defined as:

$$R = \sqrt{\frac{1}{n} \sum_{i=1}^n z_i^2}$$

where n is the number of pixels and z_i is the height of pixel i of the AFM image. Feature sizes were determined from half-width at half-maxima (HWHM) of the two-dimensional fast Fourier transform (2D-FFT) of the flattened scan, where the reciprocal of the HWHM gives a measure of the average feature size along [110] (i.e., parallel to the Si miscut direction) and [1–10] (i.e., perpendicular to the Si miscut direction). This procedure was repeated for four different areas on the surface of each sample, and the four measurements were averaged, unless stated otherwise. The standard error of the mean from the four measurements was used to define the error bars of our measurements. Analysis was carried out using MATLAB 2016b (MATLAB script available in the depository linked in the [supplementary data](#) section).

For the structural electron microscopy analysis, cross-sectional thin foils were prepared using a FEI Helios NanoLab™ focused ion beam (FIB) for in-situ lift-off. First, a 1 μm-thick Pt metal was deposited to protect the surface, followed by Ga ion milling at 30 kV and a final 5 kV treatment to reduce ion damage to make a lamella of about 80 nm to 120 nm in thickness. Scanning electron diffraction (SED) measurements were performed at FEI Technai F20 microscope operated at 200 kV in STEM mode with a NanoMegas DigiSTAR diffraction system and processed using software package Pyxem [42]. SED phase maps were

generated by matching the measured diffraction patterns at each pixel ($3 \text{ nm} \times 3 \text{ nm}$) against simulated diffraction patterns for both the zb- and the wz-GaN phases. The pixels that had a poor fitting with the simulated diffraction patterns of both phases were defined as a third, defective phase.

3. Results

3.1. Sample set A – Temperature series

The first series of samples (set A) to be discussed consisted of 6 samples in which the epilayer growth temperature was varied between $830 \text{ }^\circ\text{C}$ and $910 \text{ }^\circ\text{C}$, in steps of $15 \text{ }^\circ\text{C}$ to $20 \text{ }^\circ\text{C}$. In this series of experiments, the V/III-ratio was kept constant at 76, which represented an intermediate value within the range of values explored in sample set B (see section below).

The surface morphology of the samples grown below $880 \text{ }^\circ\text{C}$ is characterized by elongated features or striations, as shown in the Nomarski (differential interference contrast) micrographs in Fig. 1. The striations are aligned along $[1\bar{1}0]$, i.e., in the direction perpendicular to the substrate's miscut indicating an in-plane anisotropy. The length of the features shortens to a few micrometers in length with increasing temperature. At $895 \text{ }^\circ\text{C}$ and above, the surface becomes more granular and rougher with increasing temperature.

Typical AFM images of the samples of set A are shown in Fig. 2. The AFM analysis of the samples allowed a quantitative comparison of data such as the rms roughness (Fig. 3a) and in-plane dimensions of the surface features (Fig. 3b). Fig. 3a clearly shows a minimum in surface roughness of about 8 nm for samples grown at $860 \text{ }^\circ\text{C}$ and $880 \text{ }^\circ\text{C}$. As shown in Fig. 3b, the surfaces of samples grown in the lower temperature range consisted of elongated surface features a few μm in length perpendicular to the miscut direction and sub- μm parallel to it. With increasing growth temperature, above $880 \text{ }^\circ\text{C}$ the surface roughness increases quickly while the surface features gradually become more isotropic. The surface of the sample grown at $910 \text{ }^\circ\text{C}$ consists of approximately isotropic features circa $1.5 \mu\text{m}$ in size (Fig. 3b) with a (high) rms roughness reaching almost 80 nm (Fig. 3a).

To determine the phase purity of the GaN films, X-ray reciprocal space maps (RSMs) around the 113 (respectively 1–13) zb-GaN and 1–103 wz-GaN reflections were measured in both parallel and perpendicular to the 3C-SiC/Si substrate miscut direction as wz inclusions were expected to form on the four $\{111\}$ facets. The XRD analysis results of two samples, displayed in Fig. 4, will be discussed in more detail; the sample grown at $860 \text{ }^\circ\text{C}$ shows a high zincblende phase purity, as can be seen from the intense 1–13 zb reflection measured perpendicular (Fig. 4 (a)) and parallel (Fig. 4 (b)) to the sample miscut direction. The best fit for the wz reflection at about 3.64 \AA^{-1} ($Q_{\parallel[111]}$) is within the noise level of the measured intensities, revealing a wurtzite content of 0.4% or less

when measured perpendicular and parallel to the miscut. Also, the symmetric shape of the zb-reflection indicates that the proportion of a defective phase, e.g., SF-rich zb material must be relatively low in this sample. In contrast, the sample grown at $910 \text{ }^\circ\text{C}$ (Fig. 4 (c)) shows a distinct, although broad 1–103 wz reflection measured perpendicular to the miscut. This reflection is much broader than the zb reflection for all samples in this series, indicating the presence of inclusions with a poorly defined wurtzite lattice. This is likely caused by small but widely distributed hexagonal regions in the thin film. The fitting component located between the wz and zb reflections in Fig. 4 (c) is attributed to material with a defective phase and presumably composed of thin, alternating zb and wz lamella or regions with a high SF density. When measured parallel to $[110]$, the wurtzite reflection is within the noise level of the measured intensity for the sample grown at $910 \text{ }^\circ\text{C}$ (Fig. 4 (d)). It is a general observation for all samples in set A that the fitted wurtzite peak is below the detection limit, which is about 0.3%, and the contribution of highly defective material to the intensity profile is very low ($<1\%$) when measured in the direction parallel to the miscut direction. Hence, the zincblende phase purity measured in the $[110]$ direction is very high for the set A samples and independent of the epi growth temperature when grown at a pressure of 300 Torr and V/III-ratio of 76. In contrast, when measured perpendicular to the miscut direction the XRD analysis of the samples in set A revealed that the wz fraction gradually increased from $\sim 0\%$ at the lowest growth temperature to 5% at the highest temperature, as shown in Fig. 5(a). The ω -FWHM of the 002 rocking curves measured parallel and perpendicular to the miscut are shown in Fig. 5(b). The peak width decreased gradually with increasing growth temperature. For all samples, the broadening parallel to the miscut is larger than that perpendicular to the miscut. The difference between the values measured in the two in-plane directions reduces with increasing growth temperature.

To summarise the AFM and XRD characterisation of sample set A in which the epilayer growth temperature was varied at a constant V/III-ratio of 76: the film surface is relatively smooth up to a temperature of $880 \text{ }^\circ\text{C}$, consisting of μm -sized elongated features aligned along $[1\bar{1}0]$. The phase purity of the films grown at lower temperatures was high with a wz fraction of $<1\%$. At higher growth temperatures, the surface degraded and the wz fraction increased to a value of 5% for growth at $910 \text{ }^\circ\text{C}$. Wurtzite inclusions were found to be preferentially oriented with their basal planes parallel to two of the four $\{111\}$ planes in zb-GaN. The narrowing of the 002 reflection with increasing growth temperature indicates an improvement in the layers' mosaicity [34], while the 002 peak broadening perpendicular to $[110]$ is consistently smaller than that parallel to it.

3.2. Sample set B –V/III-ratio series

The second series of samples (set B) consisted of eight samples in

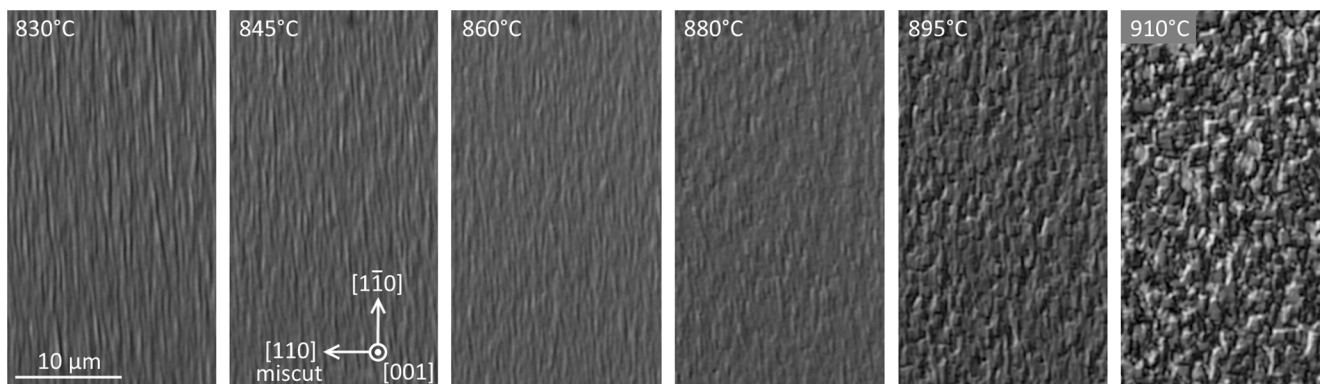


Fig. 1. Nomarski optical micrographs showing the surface of zb-GaN films grown over the temperature range of $830 \text{ }^\circ\text{C}$ to $910 \text{ }^\circ\text{C}$ at a constant V/III-ratio of 76 and a pressure of 300 Torr.

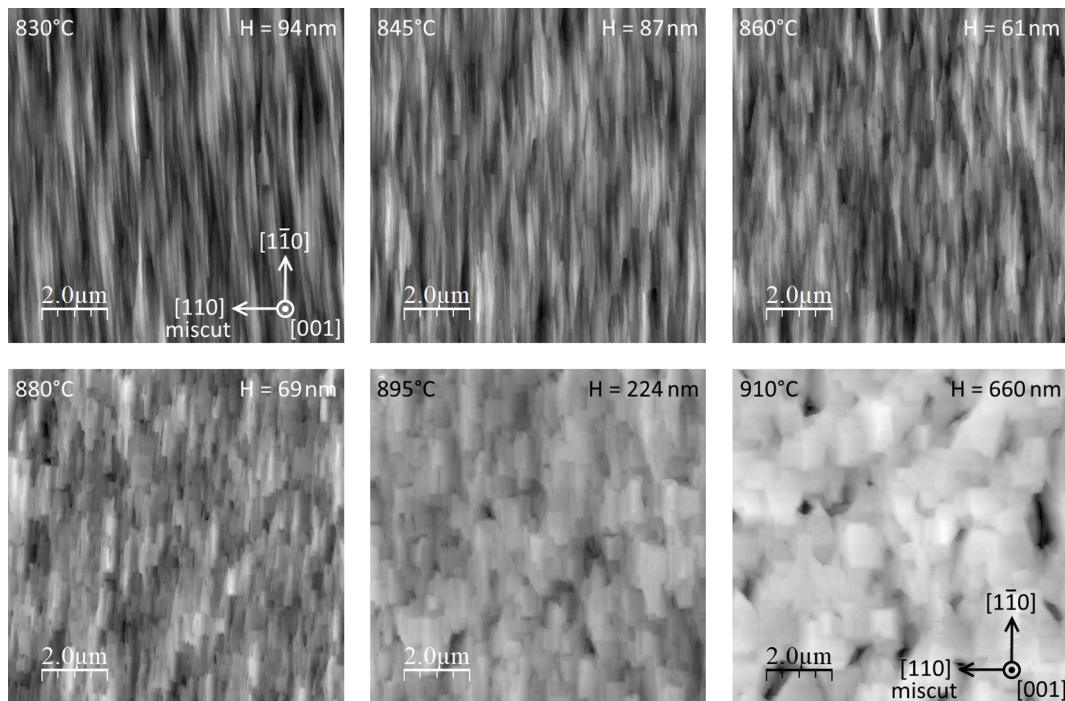


Fig. 2. AFM scans ($10 \times 10 \mu\text{m}^2$) of zb-GaN films grown over the temperature range of 830 °C to 910 °C at a constant V/III-ratio of 76 and a pressure of 300 Torr. The peak-to-valley height (H) is shown in each scan.

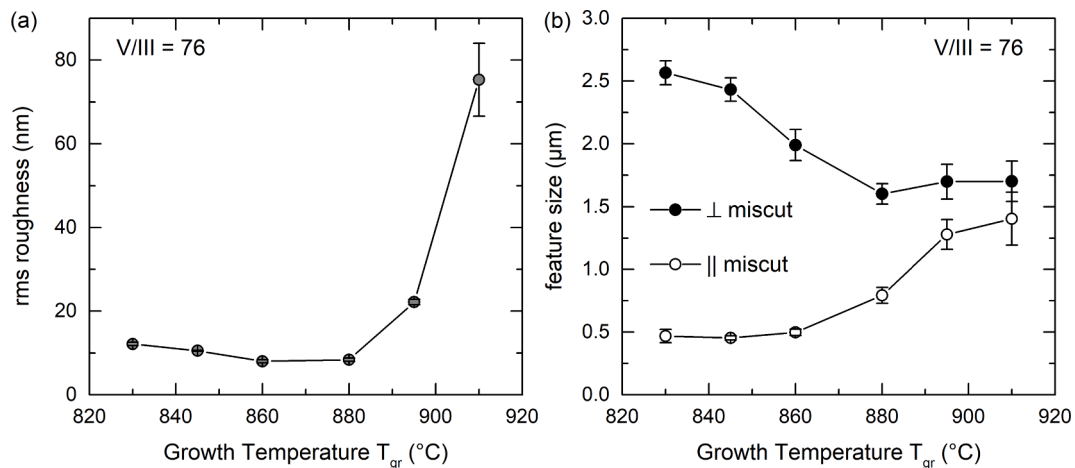


Fig. 3. The effect of epi growth temperature on (a) rms roughness, and feature size (b) parallel and perpendicular to the miscut direction $[1\bar{1}0]$ of the zb-GaN epilayers grown at a constant V/III-ratio of 76 and a pressure of 300 Torr.

which the epilayer growth temperature was kept constant at 880 °C, i.e., an intermediate value of set A, while the gas phase V/III-ratio was varied from 15 to 1200, with a factor of about two between each value. The Nomarski optical micrographs in Fig. 6 show the variation in surface morphology with increasing V/III-ratio revealing a trend that goes from granular to striated, and to granular again.

For the quantitative comparison of the surface morphology, AFM images were taken and typical images of the samples of set B are shown in Fig. 7. As in the Nomarski optical micrographs (Fig. 6), the AFM data show that the effect of the gas phase V/III-ratio on the zb-GaN surface morphology is significant. The features' dimensions are comparable to those in the temperature series (set A). The smoothest surface, consisting of elongated surface features, was obtained at a V/III-ratio of 38, with a rms-roughness of (9.7 ± 0.1) nm. Substantial deviations in surface morphology and roughness occurred away from this optimum V/III-ratio, as shown in Fig. 8. At a V/III value of 15, low aspect ratio

features were observed. The ends of these features in the $[1\bar{1}0]$ direction are poorly defined, and many include circa 50 nm-deep holes. The minimum feature length in the $[1\bar{1}0]$ direction occurs at a V/III-ratio of 76, and is approximately half the value of that obtained at either end of the investigated range, as shown in Fig. 8 (b). The maximum feature size in the $[1\bar{1}0]$ direction occurs at a V/III-ratio of 300 and is thrice that at the extremes of the investigated V/III-ratio range.

The increasing fraction of wz-type inclusions in the zb-GaN thin film when grown at a higher V/III-ratio is measured by the XRD analysis of the samples of set B, an example of which is shown in Fig. 9 for the growth at a V/III-ratio of 600. The intense $1\text{-}13_{zb}$ reflection measured perpendicular to the miscut direction (Fig. 9 (a)) is accompanied by a sharp wz reflection and a broad component in between the peaks assigned to defective material. Compared to the X-ray reflections of samples grown at V/III-ratios below 600 in this series and those of set A the wz reflection is significantly sharper which may be consistent with

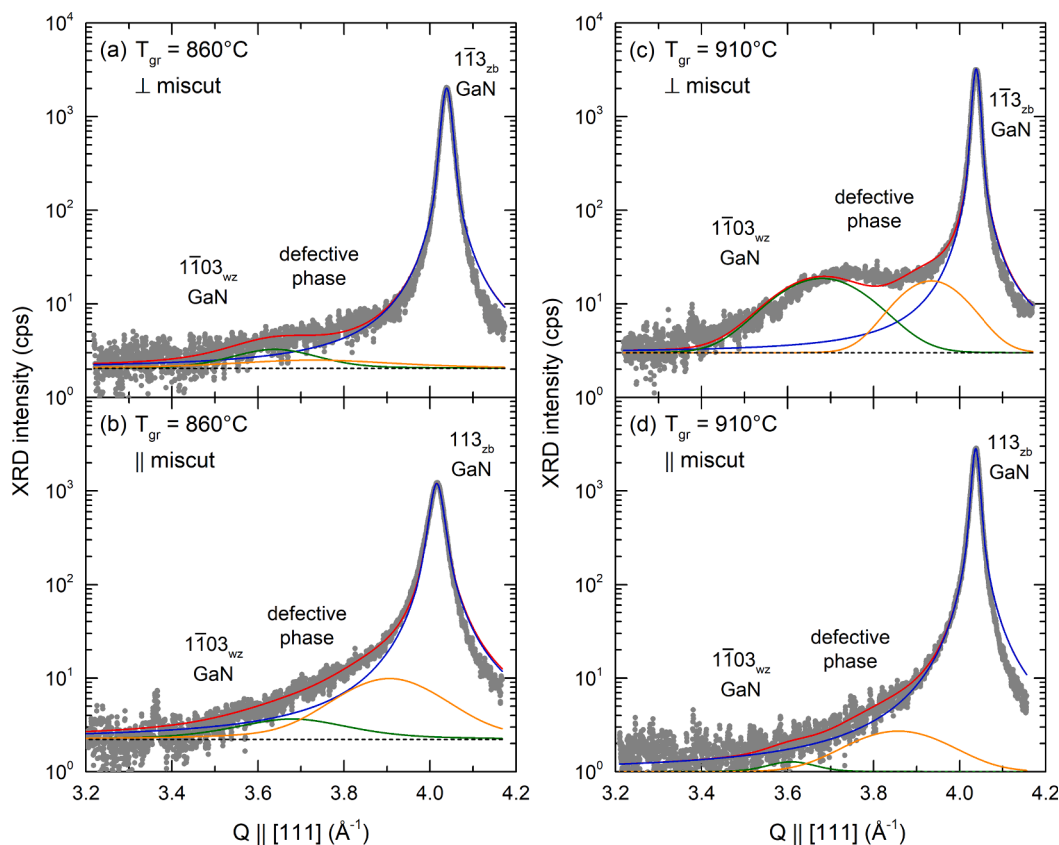


Fig. 4. XRD intensity profiles along the (111) SF streaks through the $1\bar{1}03_{wz}$ and 113_{zb} reflections for the GaN epilayers grown at a constant V/III-ratio of 76, a pressure of 300 Torr and a temperature of (a, b) 860 °C and (c, d) 910 °C measured (a, c) perpendicular and (b, d) parallel to the miscut direction [110] of the substrate. The integrated intensity of Pseudo-Voigt fits for the wz phase (green), zb phase (blue), defective phase (orange) and the total intensity (red) were used for the quantified phase analysis. (For interpretation of the references to colour in this figure legend, the reader is referred to the web version of this article.)

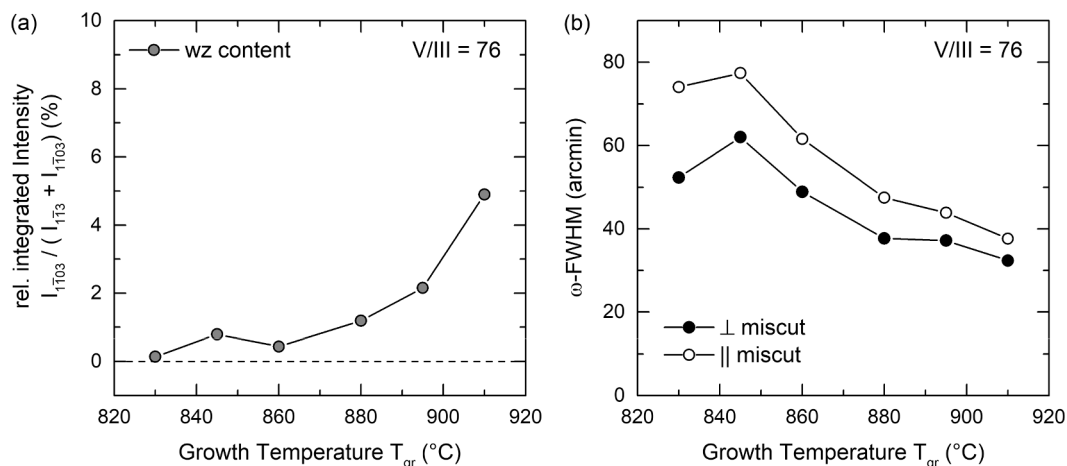


Fig. 5. (a) Wurtzite fraction from XRD and (b) XRD 002 ω -rocking curve FWHM values for GaN epilayers grown as a function of growth temperature at a constant V/III value of 76 and pressure of 300 Torr.

the presence of larger wz inclusions. As illustrated for this particular sample in Fig. 9(b), the wz reflection was within the noise level of the measured intensity in the measurement parallel to the miscut direction [110]. This was the case for all samples of set B as was observed for those of set A (see Fig. 4(b) and (d)).

More generally, the XRD phase analysis of sample set B indicates a steady increase of the wz fraction from < 1% at a V/III value of 15 to 10% at a V/III value of 600 when measured perpendicular to the miscut, as is shown in Fig. 10 (a). At the highest V/III-ratio of 1200, the wz

fraction has increased significantly to almost 60%. No significant presence of the wz phase was found in any of the samples of set B when measured parallel to the miscut direction, suggesting that wz inclusions were preferentially formed with their basal planes parallel to only two of the four {111} planes. As shown in Fig. 10(b), the ω -FWHM of the 002 rocking curves measured parallel and perpendicular to the miscut direction reveals a gradual peak broadening with increasing V/III-ratio, indicating a decrease in material quality of the zb-GaN phase. As was observed for the samples of set A (in Fig. 5(b)), the broadening parallel

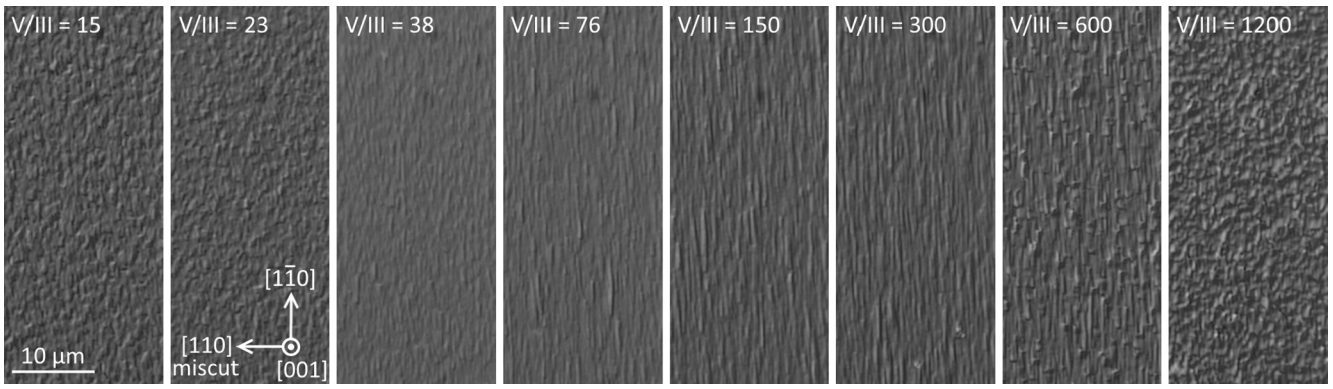


Fig. 6. Nomarski optical micrographs showing the surface of GaN epilayers grown over the V/III-range of 15 to 1200 at a constant epi growth temperature of 880 °C and pressure of 300 Torr.

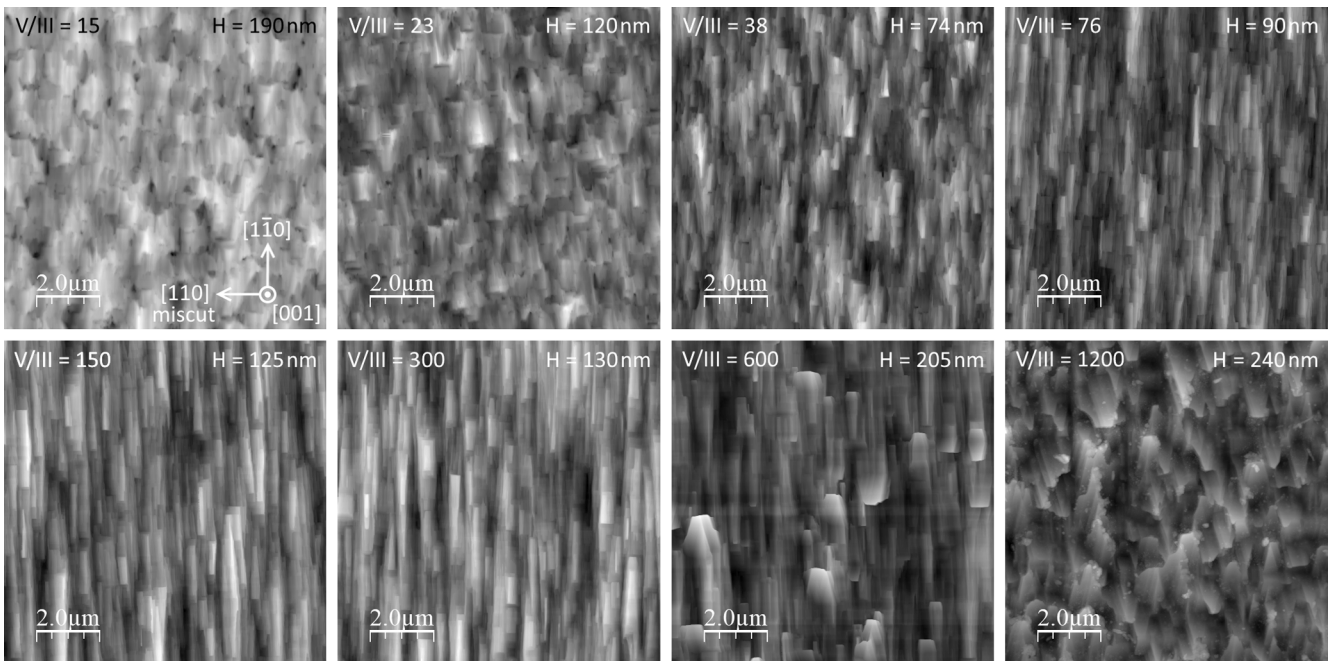


Fig. 7. AFM scans ($10 \times 10 \mu\text{m}^2$) of zb-GaN films grown at 880 °C and a V/III-ratio ranging from 15 to 1200. The peak-to-valley height (H) is shown in each scan.

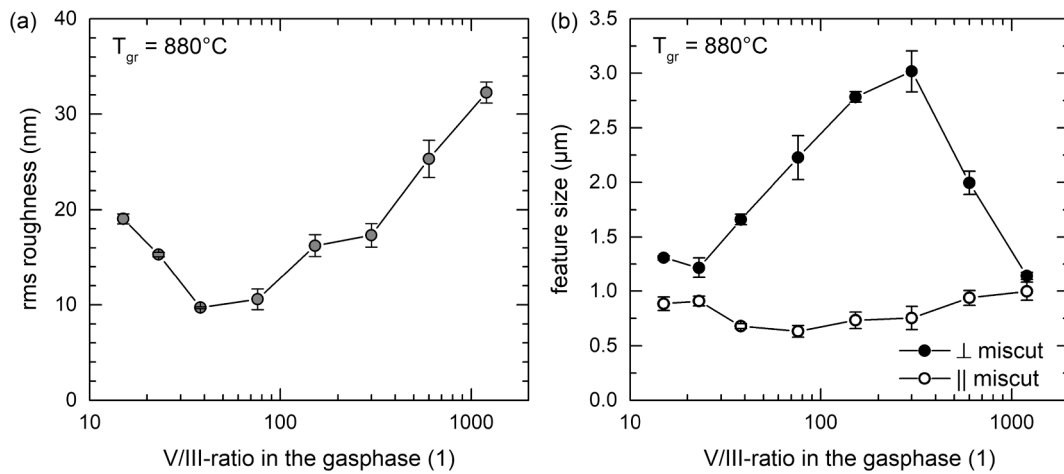


Fig. 8. The effect of V/III-ratio of GaN epilayer growth at 880 °C on a) rms roughness, and feature size b) parallel and perpendicular to the miscut direction [1 1 0].

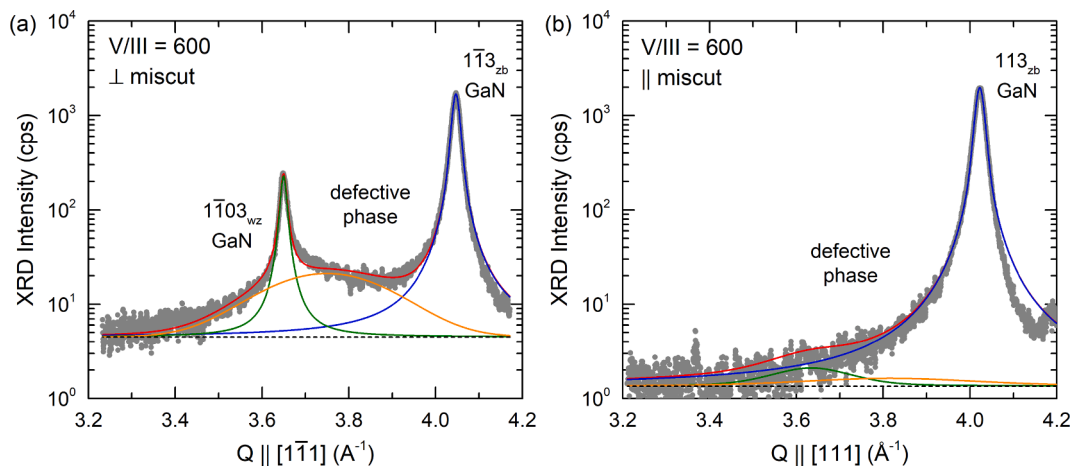


Fig. 9. XRD intensity profiles along the $\{111\}$ SF streaks through the $1\text{-}103_{wz}$ and 113_{zb} reflections for the GaN epilayer grown at 880°C and a V/III-ratio of 600 measured (a) perpendicular (b) parallel to the miscut direction of the substrate. The integrated intensity of Pseudo-Voigt fits for the wz phase (green), zb phase (blue), defective phase (orange) and the total intensity (red) were used for the phase analysis. (For interpretation of the references to colour in this figure legend, the reader is referred to the web version of this article.)

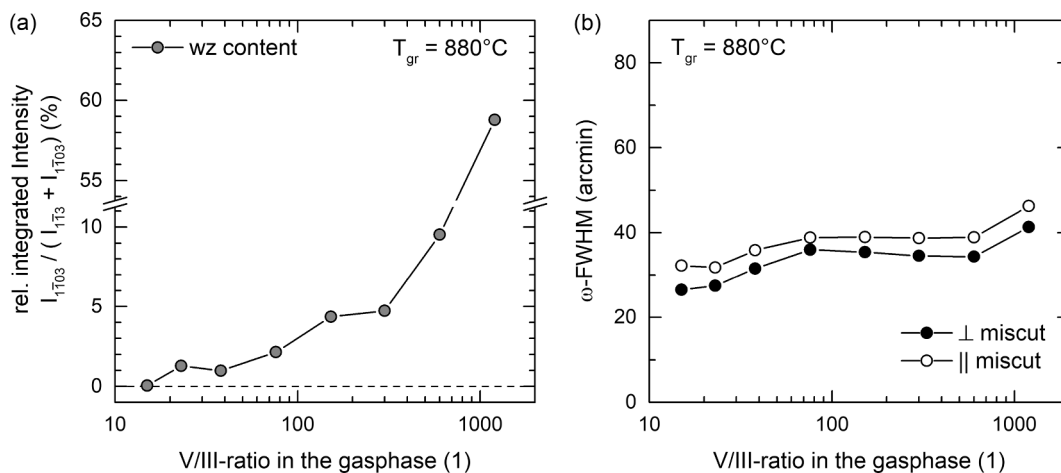


Fig. 10. (a) Wurtzite fraction from XRD, and (b) XRD 002 ω -rocking curve FWHM values for GaN epilayers grown as a function of the gas phase V/III-ratio in the MOVPE reactor at a constant temperature of 880°C and pressure of 300 Torr.

to $[110]$ is larger than that along $[1\text{-}10]$.

To visualize the changing microstructure of the GaN epilayers and in particular the structure and distribution of the increasing wz fraction with increasing gas phase V/III-ratio, Fig. 11 shows SED measurements on cross-sectional TEM foils (zone axis $[110]$) prepared from set B samples grown at V/III ratios of (a) 15, (b) 300 and (c) 1200, coinciding with wz contents of $< 1\%$, 5% and 60% , respectively, as measured by XRD. The micrograph in Fig. 11(a) shows a cross-section of the GaN epilayer with the zb phase (false-coloured green) with only a few small wz (false-coloured red) and defective areas (false-coloured yellow). The locations with a defective or wz phase within the GaN film form thin lines following the $\{111\}$ crystallographic planes and hence associated with SFs in zb-GaN. Near the top centre of the image in Fig. 11(a) is visible a diagonal red line which represents a thin slab of wz material that was formed on the $\{111\}$ facet but did not significantly grow in thickness under the specific reactor conditions used. The low fraction of red-coloured wz material in the micrograph in Fig. 11(a) agrees with XRD phase analysis measurements of this sample. In Fig. 11(b), the SED image of the GaN layer grown at a V/III-ratio of 300 shows red-coloured bands of wz inclusions, which thread diagonally through almost the entire thickness of the epilayer. Clearly, the higher ammonia flow during growth favoured the formation of the wz phase in the $\langle 111 \rangle$ direction,

possibly nucleating from areas of SFs or surface features with growing $\{111\}$ facets. When grown at the still higher V/III-ratio of 1200, large areas of the GaN film are of the wz phase as shown in Fig. 11(c). The high fraction of red-coloured wz material in this particular sample also agrees with XRD phase analysis measurements. It is interesting to note that along the length of the micrographs shown in Fig. 11 the first ca. 100 nm of epigrowth is largely zincblende in phase suggesting that $\{111\}$ facets at the surface take some time to develop before acting as wz nucleation sites.

To summarise the characterisation data of sample set B in which the gas phase V/III-ratio was varied at a constant epilayer growth temperature of 880°C : the film surface is relatively smooth between values 23 and 150, consisting of $\mu\text{-sized}$ elongated features aligned along $[1\text{-}10]$, i.e., perpendicular to the miscut direction. The zb phase purity is high but deteriorates rapidly at V/III values higher than 300. The slight broadening of the 002 reflection with increasing V/III-ratio indicates small degradation of the mosaicity, while the 002 peak broadening parallel to $[110]$ is consistently greater than that perpendicular to it. SED measurements on cross-sectional TEM samples (with $[110]$ zone axis) show the increasing propensity for nucleation of wz inclusions running parallel to the $\{111\}$ planes in zb-GaN with increasing V/III values during film growth. The TEM data confirm that the wz phase is

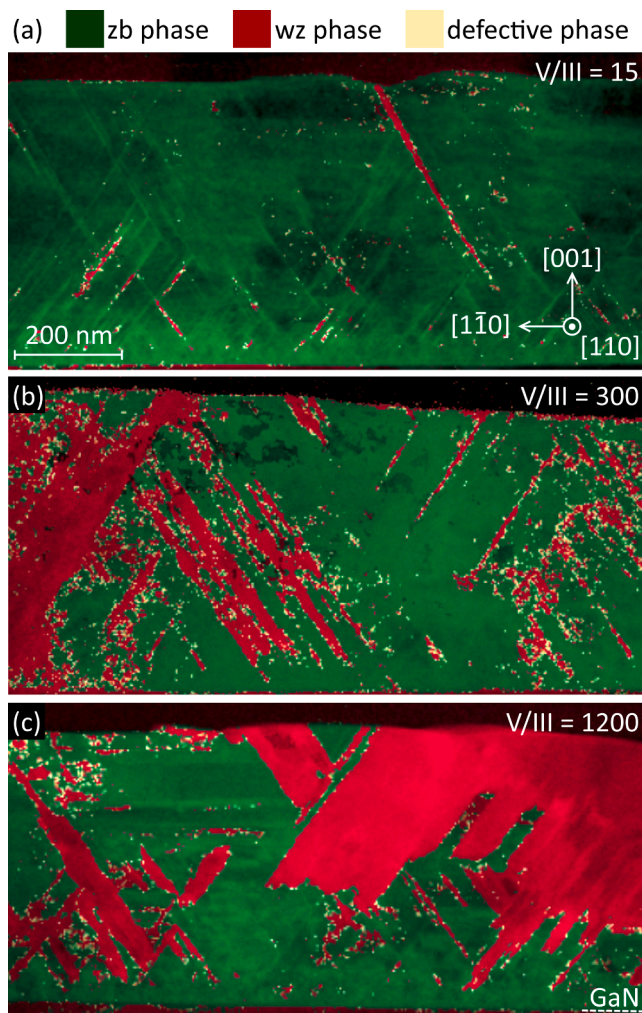


Fig. 11. SED phase maps (zone axis $[110]$) for three GaN samples of set B grown at $880\text{ }^{\circ}\text{C}$, 300 Torr and a V/III-ratio of a) 15, b) 300, and c) 1200, showing zincblende regions in green and wurtzite regions in red. Areas of poor fitting are shown in yellow, and defined as a defective phase. (For interpretation of the references to colour in this figure legend, the reader is referred to the web version of this article.)

effectively suppressed during GaN epi growth at a low V/III value.

4. Discussion

The structural data of sample set A in which the temperature was varied at a constant V/III-ratio reveal that films grown with a V/III of 76 and a growth temperature between $860\text{ }^{\circ}\text{C}$ and $880\text{ }^{\circ}\text{C}$ have relatively smooth surfaces with a high phase purity. Although the fraction of wz contamination gradually increases with growth temperature, there is no obvious correlation with the AFM-measured surface roughness. The sample grown at $910\text{ }^{\circ}\text{C}$ stands out because of its rough morphology, but this did not lead to a sudden rise in wz-GaN incorporation. The only metric consistently improving with growth temperature is the mosaicity of the zb-GaN film, as inferred from the narrowing of the 002 reflection by a factor of two over the studied temperature range. Considering an epi layer with low roughness and low wz contamination to be favoured over one with a better structural mosaicity, the target growth temperature lies between 860 and $880\text{ }^{\circ}\text{C}$ when grown at 300 Torr and at a V/III-ratio of 76.

The characterisation of sample set B in which the V/III-ratio was varied at a constant growth temperature of $880\text{ }^{\circ}\text{C}$ further aided the exploration for suitable growth conditions. At the extremes of the

studied V/III range (see Figs. 6 and 7), the surfaces are granular while the smoothest surface is observed for the sample grown at a V/III-ratio of 38. The wz-GaN contamination is insignificant for the samples with gas phase V/III-ratio of 15 and 23, despite their relatively rough surfaces (cf. Figs. 8 and 10a). It is tempting to correlate the gradual rise in wz contamination with a worsening of the surface morphology with higher V/III-ratio, although this trend was not confirmed from the data of set A. It has been suggested that the formation of $\{111\}$ facets enhances nucleation and growth of the wurtzite phase [3,39], although the crystallography of the surface facets in our samples could not be confirmed. If this were the case, however, the type of faceted surface of the samples at a V/III-ratio below 38 must be distinctly different in crystallography as the XRD analysis showed it did not lead to wz-GaN formation.

At a thickness of 500 nm the film grown under such conditions has ω -FWHM values of the 002 reflection as low as 31 arcmin and 36 arcmin, measured perpendicular and parallel to the direction of the 4° miscut respectively. These rocking curve values also represent the state-of-the-art for zb-GaN film when compared with the literature data from MBE- and MOVPE-grown films on the different substrates (see ref. 34 and cited references).

A comparison with previously reported data from our group [8] allows further examination of the effect of growth pressure for control of the zb-GaN phase purity. Fig. 12 illustrates the difference in wz fraction as a function of growth temperature (Fig. 12(a)) and V/III-ratio (Fig. 12 (b)) at a reactor pressure of 300 Torr in comparison to a significantly different pressure (as used in Ref. [8]). The trends of wz content with changing epi temperature and V/III-ratio are shown to be very similar including the undesired wz phase that forms at high temperatures and V/III-ratios, possibly due to a preference for $\{111\}$ surface facets under these conditions. These observations suggest that the reactor pressure is not a significant parameter to achieve high phase purities.

The XRD data shown in Fig. 4 (c) and (d) revealed distinct anisotropy of wz inclusions in the sample that was grown at $910\text{ }^{\circ}\text{C}$. The XRD data in Fig. 9 showed the same phenomenon occurred in samples that were grown at high V/III values. Hence, at epilayer growth temperatures and V/III ratios above their optimal values, significant amount of wurtzite GaN was formed on $\{111\}$ facets oriented perpendicular to the miscut direction $[110]$ of the substrate. On the other hand, the XRD analysis showed that no relevant wurtzite formation was observed on $\{111\}$ facets tilted parallel to the miscut direction $[110]$. In accordance with the XRD observations, the SED image of Fig. 11 (c) confirms the presence of wurtzite crystals formed on $\{111\}$ facets perpendicular to the miscut direction $[110]$, which was selected to be the same direction as the zone axis of the image. The anisotropy of wz-phase inclusions is likely the result of preferential wz nucleation on Ga-face over N-face $\{111\}$ facets under the growth conditions specified above, and this will be the subject of a separate publication [43].

5. Conclusions

Cubic zb-GaN epilayers were grown successfully by MOVPE on 3C-SiC/Si(111) templates. The epilayer growth temperature and V/III ratio were varied in two series of samples, with otherwise fixed conditions for the high-temperature preparation of the substrate and the low-temperature nucleation layer deposition. Considering the collective data of surface morphology, phase purity and film mosaicity of the two sample sets, the optimum MOVPE growth conditions at a constant pressure of 300 Torr are found at a relatively narrow temperature window from $860\text{ }^{\circ}\text{C}$ to $880\text{ }^{\circ}\text{C}$ and a V/III ratio range between ~ 20 and 80, resulting in a relatively smooth zb-GaN film with a phase purity of $> 99\%$. This process window is similar to that observed for a different reactor pressure [8] which suggests that the reactor pressure for epilayer growth is a non-critical process parameter.

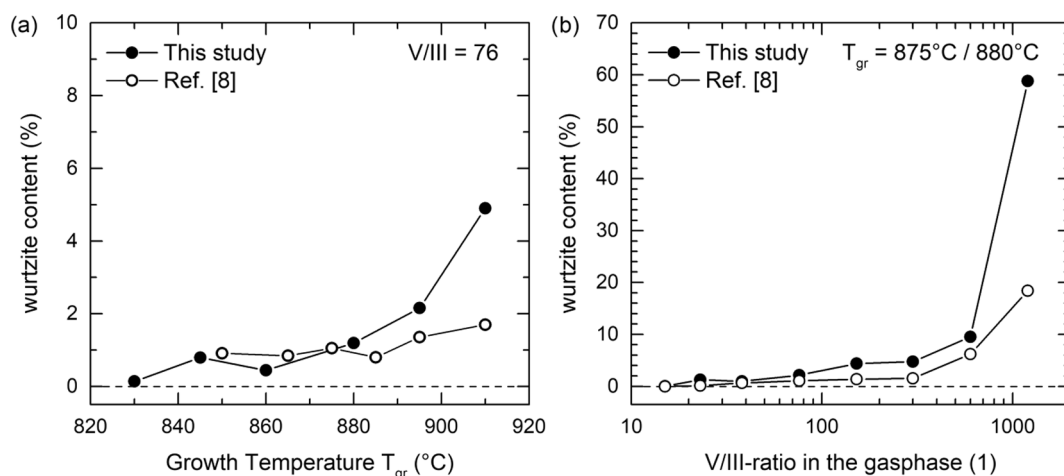


Fig. 12. Wurtzite fraction determined by XRD in zb-GaN epilayers grown at two different reactor pressures as a function at temperature (a) and V/III ratio (b). The temperature-dependent samples in (a) were all grown at a constant V/III-ratio of 76; while the V/III-dependent samples in (b) were grown at 875 °C (Ref. [8]) and 880 °C (this study).

CRediT authorship contribution statement

T.J. Wade: Validation, Investigation, Writing - original draft. **A. Gundimeda:** Validation, Formal analysis, Investigation. **M.J. Kappers:** Conceptualization, Methodology, Validation, Investigation, Writing - original draft, Writing - review & editing. **M. Frentrop:** Conceptualization, Methodology, Validation, Investigation, Writing - original draft, Writing - review & editing. **S.M. Fairclough:** Software, Validation, Formal analysis, Investigation. **D.J. Wallis:** Conceptualization, Validation, Funding acquisition, Writing - review & editing. **R.A. Oliver:** Conceptualization, Validation, Funding acquisition, Writing - review & editing.

Declaration of Competing Interest

The authors declare the following financial interests/personal relationships which may be considered as potential competing interests: Rachel A. Oliver reports financial support was provided by Engineering and Physical Sciences Research Council. David J. Wallis reports financial support was provided by Innovate UK. David J. Wallis reports financial support was provided by Engineering and Physical Sciences Research Council.

Data availability

Data will be made available on request.

Acknowledgments

This work was enabled through financial support by Innovate UK through the Energy Catalyst Round 2 - Early Stage Feasibility scheme (Ref. 132135): "To demonstrate the potential to make low cost, high efficiency LEDs using 3C-SiC substrates", and by EPSRC through platform grant no. EP/M010589/1: "Beyond Blue: New Horizons in Nitrides". D J Wallis would like to thank the support of EPSRC through grant no. EP/N01202X/1.

Appendix A. Supplementary data

Supplementary data to this article can be found online at <https://doi.org/10.1016/j.jcrysgro.2023.127182>.

References

- [1] H. Okumura, K. Ohta, G. Feuillet, K. Balakrishnan, S. Chichibu, H. Hamaguchi, P. Hacke, S. Yoshida, *J. Cryst. Growth* 178 (1997) 113.
- [2] O. Brandt, Ch. 11 in *Group III nitride semiconductor compounds: physics and applications*, in: B. Gil (Ed.), Oxford: Clarendon Press; New York: Oxford University Press, 1998.
- [3] B. Daudin, G. Feuillet, J. Hübner, Y. Samson, F. Widmann, A. Philippe, C. Bru-Chevallier, G. Guillot, E. Bustarret, G. Bentoumi, A. Deneuve, *J. Appl. Phys.* 84 (1998) 2295.
- [4] D.J. As, D. Schikora, K. Lischka, *Phys. Stat. Sol. (C)* (2003) 1607.
- [5] D.J. As, Proc. of SPIE Vol. 7608, *Quantum Sensing and Nanophotonic Devices VII*; 76080G-15, 2010.
- [6] A. Nakadaira, H. Tanaka, *J. Electron. Mater.* 26 (1997) 320.
- [7] J. Wu, H. Yaguchi, H. Nagasawa, Y. Yamaguchi, K. Onabe, Y. Shiraki, R. Ito, *Jpn. J. Appl. Phys.* 36 (1997) 4241.
- [8] L.Y. Lee, M. Frentrop, M.J. Kappers, R.A. Oliver, C.J. Humphreys, D.J. Wallis, *J. Appl. Phys.* 124 (2018), 105302.
- [9] C.J.M. Stark, T. Detchprohm, S.C. Lee, Y.-B. Jiang, S.R.J. Brueck, C. Wetzel, *Appl. Phys. Lett.* 103 (2013), 232107.
- [10] C. Bayram, J.A. Ott, K.-T. Shiu, C.-W. Cheng, Y. Zhu, J. Kim, M. Razeghi, D. K. Sadana, *Adv. Funct. Mater.* 24 (2014) 4492.
- [11] M.T. Durniak, A.S. Bross, D. Elsaesser, A. Chaudhuri, M.L. Smith, A.A. Allerman, S. C. Lee, S.R.J. Brueck, C. Wetzel, *Adv. Electron. Mater.* 2 (2016) 1500327.
- [12] R. Liu, C. Bayram, *Appl. Phys. Lett.* 109 (2016), 042103.
- [13] S.F. Chichibu, M. Sugiyama, T. Onuma, T. Kitamura, H. Nakanishi, T. Kuroda, A. Takeuchi, T. Sota, Y. Ishida, H. Okumura, *Appl. Phys. Lett.* 79 (2001) 4319.
- [14] S. Li, J. Schörmann, D.J. As, K. Lischka, *Appl. Phys. Lett.* 90 (2007), 071903.
- [15] D.J. As, *J. Microelectronics* 40 (2009) 204.
- [16] D.R. Elsaesser, M.T. Durniak, A.S. Bross, C. Wetzel, *J. Appl. Phys.* 122 (2017), 115703.
- [17] M.E. Lin, G. Xue, G.L. Zhou, J.E. Greene, H. Morkoç, *Appl. Phys. Lett.* 63 (1993) 932.
- [18] J.W. Orton, C.T. Foxon, *Rep. Prog. Phys.* 61 (1998) 1.
- [19] D.J. As, *Phys. Stat. Sol. (B)* 210 (1998) 445.
- [20] D.J. As, K. Lischka, *Phys. Stat. Sol. (A)* 176 (1999) 475.
- [21] E. Martinez-Guerrero, B. Daudin, G. Feuillet, H. Mariette, Y. Genuist, S. Fanget, A. Philippe, C. Dubois, C. Bru-Chevallier, G. Guillot, P. Aboughe Nze, T. Chassagne, Y. Monteil, H. Gamez-Cuatzin, J. Tardy, *Mat. Sci. Eng.* B82 (2001) 59.
- [22] D. Xu, H. Yang, J.B. Li, S.F. Li, Y.T. Wang, D.G. Zhao, R.H. Wu, *J. Cryst. Growth* 206 (1999) 150.
- [23] H. Vilchis, V.M. Sánchez-R, *Mater. Sci. Semicond. Process.* 37 (2015) 68.
- [24] V.D. Compeán-García, H. Moreno-García, E. López-Luna, H. Pérez Ladrón de Guevara, A. Escobosa Echavarría, Y. Kudriatsev, F.J. Rodríguez-Aranda, A. G. Rodríguez, M.A. Vidal, *Mater. Sci. Semicond. Process.* 93 (2019) 196.
- [25] E.A. Hernandez-Gutierrez, Y.L. Casallas-Moreno, V.-T. Rangel-Kuoppa, D. Cardona, Y. Hu, Y. Kudriatsev, M.A. Zambrano-Serrano, S. Gallardo-Hernandez, M. Lopez-Lopez, *Sci. Rep.* 10 (2020) 16858.
- [26] H. Yang, L.X. Zheng, J.B. Li, X.J. Wang, D.P. Xu, Y.T. Wang, X.W. Hu, P.D. Han, *Appl. Phys. Lett.* 74 (1999) 2498.
- [27] H. Gamez-Cuatzin, J. Tardy, P. Rojo-Romeo, A. Philippe, C. Bru-Chevallier, A. Souifi, G. Guillot, E. Martinez-Guerrero, G. Feuillet, B. Daudin, P. Aboughe-Nzé, Y. Monteil, *Phys. Stat. Sol. (A)* 176 (1999) 131.
- [28] D.J. As, A. Richter, J. Busch, M. Lübbbers, J. Mimkes, K. Lischka, *Appl. Phys. Lett.* 76 (2000) 13.
- [29] Y. Taniyasu, K. Suzuki, D.H. Lim, A.W. Jia, M. Shimotomai, Y. Kato, M. Kobayashi, A. Yoshikawa, K. Takahashi, *Phys. Stat. Sol. (A)* 180 (2000) 241.

- [30] S.C. Lee, X.Y. Sun, S.D. Hersee, S.R.J. Brueck, H. Xu, *Appl. Phys. Lett.* 84 (2004) 2079.
- [31] J. Wu, H. Yaguchi, K. Onabe, R. Ito, Y. Shiraki, *Appl. Phys. Lett.* 71 (1997) 2067.
- [32] J. Wu, H. Yaguchi, H. Nagasawa, Y. Yamaguchi, K. Onabe, Y. Shiraki, R. Ito, *Jpn. J. Appl. Phys.* 37 (1998) 1440.
- [33] D. Xu, H. Yang, J.B. Li, S.F. Li, Y.T. Wang, D.G. Zhao, R.H. Wu, *J. Electron. Mater.* 29 (2000) 177.
- [34] M. Frentrup, L.Y. Lee, S.-L. Sahonta, M.J. Kappers, F. Massabuau, P. Gupta, R. A. Oliver, C.J. Humphreys, D.J. Wallis, *J. Phys. D: Appl. Phys.* 50 (2017), 433002.
- [35] D. Zhu, D.J. Wallis, C.J. Humphreys, *Rep. Prog. Phys.* 76 (2013), 106501 plus references therein.
- [36] D. Gerthsen, B. Neubauer, C.h. Dieker, R. Lantier, A. Rizzi, H. Lüth, *J. Cryst. Growth* 200 (1999) 353.
- [37] J. Camassel, P. Vicente, N. Planes, J. Allègre, J. Pankove, F. Namavar, *Phys. Stat. Sol. (B)* 216 (1999) 253.
- [38] C.H. Wei, Z.Y. Xie, L.Y. Li, Q.M. Yu, J.H. Edgar, *J. Electron. Mater.* 29 (2000) 317.
- [39] R.M. Kemper, T. Schupp, M. Häberlen, T. Niendorf, H.-J. Maier, A. Dempewolf, F. Bertram, J. Christen, R. Kirste, A. Hoffmann, J. Lindner, D.J. As, *J. Appl. Phys.* 110 (2011), 123512.
- [40] L.Y. Lee, M. Frentrup, P. Vacek, M.J. Kappers, D.J. Wallis, R.A. Oliver, *J. Appl. Phys.* 125 (2019), 105303.
- [41] I. Horcas, R. Fernández, *Rev. Sci. Instr.* 78 (2007), 013705.
- [42] Scanning electron diffraction (SED) data were processed using open source Pyxem software available at doi: 10.5281/zenodo.5075520.
- [43] H. Xiu, S.M. Fairclough, A. Gundimeda, M.J. Kappers, D.J. Wallis, R.A. Oliver, M. Frentrup, *J. Appl. Phys.* (2022) submitted.